Journal of Microscopy

Journal of Microscopy, Vol. 279, Issue 3 2020, pp. 217–221
Received 1 August 2019; accepted 23 January 2020

doi: 10.1111/jmi.12869

Effect of annealing on the magnetic states of FEBID-grown cobalt nanopatterns examined by off-axis electron holography

T. ALMEIDA*, D. MCGROUTHER*, A. KOVÁCS†, R. DUNIN-BORKOWSKI† & S. MCVITIE*

*School of Physics and Astronomy, University of Glasgow, Glasgow, U.K.

†Ernst Ruska-Centre for Microscopy and Spectroscopy with Electrons (ER-C), Peter Grünberg Institute, Forschungszentrum Jülich, Jülich, Germany

Key words. Core-shell, focused electron beam-induced deposition, nanomagnetism, nanoparticles, off-axis electron holography.

Summary

The growth of cobalt nanopatterns (NPs) using focused electron-beam induced deposition (FEBID) for localised magnetic studies is presented. The initial FEBID products are shown to be polycrystalline and form hetero-structured core-shell NPs through surface oxidation. Off-axis electron holography is performed to reconstruct their morphology, thickness profile and image their individual magnetic vortex domain states. *In situ* annealing to 400°C promoted migration of the Co-overspray to grow the Co NPs and improved their crystallinity through coarsening, as well as induced diffusion of embedded carbon out of their surface. It is found that the change in their morphology and chemical instability under heating restricts their suitability for examining thermally induced magnetic variations.

Introduction

The demand for improved functionality in magnetoelectronic devices is resulting in the development of innovative combinations of hard and soft magnetic materials, which are referred to as exchange-spring magnets. In a bimagnetic core-shell (CS) nanostructure, exchange coupling across the CS interface facilitates cooperative magnetic switching and provides tuneable magnetic properties (Lee *et al.*, 2011; Lavorato *et al.*, 2015). However, our current understanding of the CS exchange interaction is limited to bulk magnetic measurements and micromagnetic modelling, driving the need for more localised studies using transmission electron microscopy (TEM) techniques. CS nanostructures are commonly synthesized as powders or dispersions through chemical routes including co-precipitation, hydrothermal synthesis, etc., but often exhibit a wide size distribution, agglomerate easily and are difficult to isolate for localized magnetic studies without inter-particle interactions (Almeida *et al.*, 2014). Modern scanning electron microscopes (SEMs) can incorporate systems for the injection of element-containing gases that can be used as precursors for creating magnetic nanopatterns (NPs), with feature sizes as small as 10 nm, using focused electron beam induced deposition (FEBID) (Serrano-Ramón *et al.*, 2011; Fernández-Pacheo *et al.*, 2013; De Teresa *et al.*, 2016). In FEBID, the electron beam is used to dissociate the precursor gas near a substrate and locally deposit the carried metal in the same shape as the scanned beam. Alteration of the electron-beam scan conditions during beam-induced decomposition of the injected gases provides effective control over the size, morphology and inter-spacing of the deposited magnetic material. Further, the deposition of reactive ferromagnetic metals such as Co (Fernández-Pacheo *et al.*, 2009; Fernández-Pacheo *et al.*, 2009; Córdoba *et al.*, 2010) can result in the formation of CS NPs through surface oxidation. Hence, we are in a timely position to synthesise isolated CS systems using FEBID and use the TEM technique of off-axis electron holography to investigate the effect of localized magnetic exchange coupling between their metal-core and oxide-shell. One useful method to induce dynamic magnetic processes that provide access to the effect of exchange coupled CS systems is through *in situ* heating. However, to isolate the effects on magnetism we must first understand the effect of heating on the original FEBID-grown CS NPs. In the present study, we investigate the effect of annealing on structural, chemical and magnetic properties of CS NPs using a series of advanced *in situ* TEM techniques.

Experimental

FEBID is used to synthesise a range of Co NPs on electron-transparent SiN membranes of DENSSolutions Wildfire^{TM} TEM electronic (e-) chips, with two Co NPs presented here (~90 nm in diameter). $Co_2(CO)_8$ was used as a precursor for the elemental deposition of Co, with the gas injection system (GIS) needle

Correspondence to: Trevor P. Almeida, School of Physics and Astronomy, University of Glasgow, Glasgow G12 8QQ, UK. Tel: +44(0)1413304712; e-mail: trevor.almeida@glasgow.ac.uk

inserted to the standard height relative to the SiN membrane located at the working distance of 3.9 mm from the SEM column pole piece. The GIS needle has a diameter of 300 μm and was positioned 70 μm from the SEM beam, at an angle of 48° relative to the optic axis. The precursor crucible was heated to 28°C prior to the start of the gas flow and the growth was controlled through systematic variation of the SEM electron beam voltages (5–15 kV) and beam currents (0.34–0.69 nA). Conventional and scanning TEM imaging of the FEBID-grown NPs was performed using a Thermo Fisher Titan G2 80–200 or Tecnai G2 F20 (both ER-C) at 200 kV, with structural analysis provided by selected area electron diffraction (SAED). Energy dispersive X-ray (EDX) spectroscopy allowed for chemical mapping of the elemental distribution across the CS NPs. Off-axis electron holograms were acquired at 300 kV in Lorentz mode in a Titan 80–300 TEM (ER-C) equipped with an image aberration corrector, rotatable electron biprisms and recorded using a Gatan K2 high-speed direct electron detection camera. The total phase shift of the electron wave recorded in one dimension, $\phi(x)$, is sensitive to the electrostatic potential, ϕ_e, and the in-plane component of the magnetic induction, ϕ_m, in the specimen, as summarised by

$$\begin{aligned}\phi(x) &= \phi_e + \phi_m \\ &= C_E \int V(x,z)\,dz - \left(\frac{2\pi e}{h}\right)\int A_z(x,z)\,dz,\end{aligned}$$

where the incident electron beam direction z is perpendicular to x, C_E is an interaction constant that takes a value of 6.53×10^6 radV^{-1}m^{-1} at an accelerating voltage of 300 kV, V is the electrostatic potential and A_z is the component of the magnetic vector potential along z. Absent from additional charge redistribution around the sample, V comprises primarily the mean inner potential (MIP) of the material V_0. If the MIP of material does not vary within its thickness t, then ϕ_e can be simplified to $\phi_e = C_E V_0 t$. Each NP was initially magnetized in opposite directions by tilting the sample by $\pm 75°$ and turning on the conventional microscope objective lens to apply a saturating magnetic field of >1.5 T. This allowed for the cancellation of the net magnetic contribution to the phase in order to determine the MIP contribution, and through subtraction of this MIP contribution the in-plane magnetic induction in one of the two tilt directions was isolated. For the purpose of examining the effect of annealing, holograms were acquired in magnetic-field-free conditions at 25°C before and after *in situ* heating to 400°C for 10 min under vacuum using the DENSSolutions Wildfire^{TM} heating holder, as described previously (Almeida *et al.*, 2016, Almeida *et al.*, 2016). For construction of the magnetic induction maps, the cosine of the magnetic contribution was amplified to produce phase contours and colours were added to show the direction of the projected induction (denoted by the colour wheels). The outlines of the NPs were determined using an appropriate threshold on the MIP contribution to the phase shift.

Results

Figure 1 presents the effect of annealing on a FEBID-grown Co NP, providing information on the changes of its size, chemical composition, localised structure, morphology and magnetisation. The bright field (BF) TEM image of Figure 1(A) provides a localised view of the native Co NP (~90 nm in diameter) at 25°C with obvious regions of Co overspray from FEBID process in its close vicinity, whilst the diffraction rings in the corresponding SAED pattern (Fig. 1A, inset) reveals the Co NP to be polycrystalline. The EDX chemical maps (Fig. 1B) show the Co distribution to be uniform across the NP but exhibits an O-rich surface layer, confirming the formation of an Co/Co-oxide CS structure. A large C signal is also detected and is considered due to embedding of residual hydrocarbon molecules remaining as a reaction product of the dissociated $Co_2(CO)_8$ precursor (Bernau *et al.*, 2010). Figure 1(C) presents the morphology and thickness profile (~110 nm maxima) of the Co NP, determined using the equation $\phi_e = C_E V_0 t$, where $V_0 = 25.0$ V is estimated by averaging several values of MIP for Co (Anishchenko, 1966; Sanchez & Ochando, 1985; Dunin-Borkowski *et al.*, 1998). Figure 1(D) displays a magnetic induction map of the Co NP and the central contours flowing from right to left could be misinterpreted as a uniformly magnetized state. However, due to its size and part of the flux loops either side of the central magnetic contours being contained within the Co NP, it is more likely to be a vortex state that is observed edge-on (Chong *et al.*, 2003, Hÿtch *et al.*, 2003). Figure 1(E) demonstrates the effect of *in situ* annealing to 400°C, revealing migration and build-up of the Co overspray on the Co NP. The EDX maps of Figure 1(F) display a pronounced O signal at the Co NP edge and depletion of 50% of total atomic C% from the NP surface, as shown in the summary of atomic % before and after annealing (Table 1). The associated morphology and thickness profile (Fig. 1G) reveal amplified overspray roughness and an increase in height of the Co NP by ~25 nm. The magnetic induction map of Figure 1(H) clearly shows a change to a vortex state flowing in a clockwise direction with a stray magnetic field.

Similar to Figure 1, Figure 2 presents the effect of annealing on the second FEBID-grown Co NP. The BF TEM image (Fig. 2A) shows a similar Co NP (~90 nm in diameter) and Co overspray, with bright spots in the SAED pattern corresponding to the {100} set of planes of Co_3O_4. The EDX chemical maps (Fig. 2B) show similar elemental distributions of Co, O and C as the Co NP in Figure 1(B), and Fig. 2(C) reveals it to be analogous in morphology but slightly thicker at ~130 nm. The magnetic induction map of Figure 2(D) clearly shows a vortex state flowing in an anti-clockwise direction. Annealing of the Co NP at 400°C again results in migration and build-up of the Co overspray (Fig. 2E), along with an increase in intensity of the diffraction spots in SAED pattern (inset), indexed to Co_3O_4. The EDX maps of Figure 2(F) display do not reveal much change in the Co NP apart from depletion

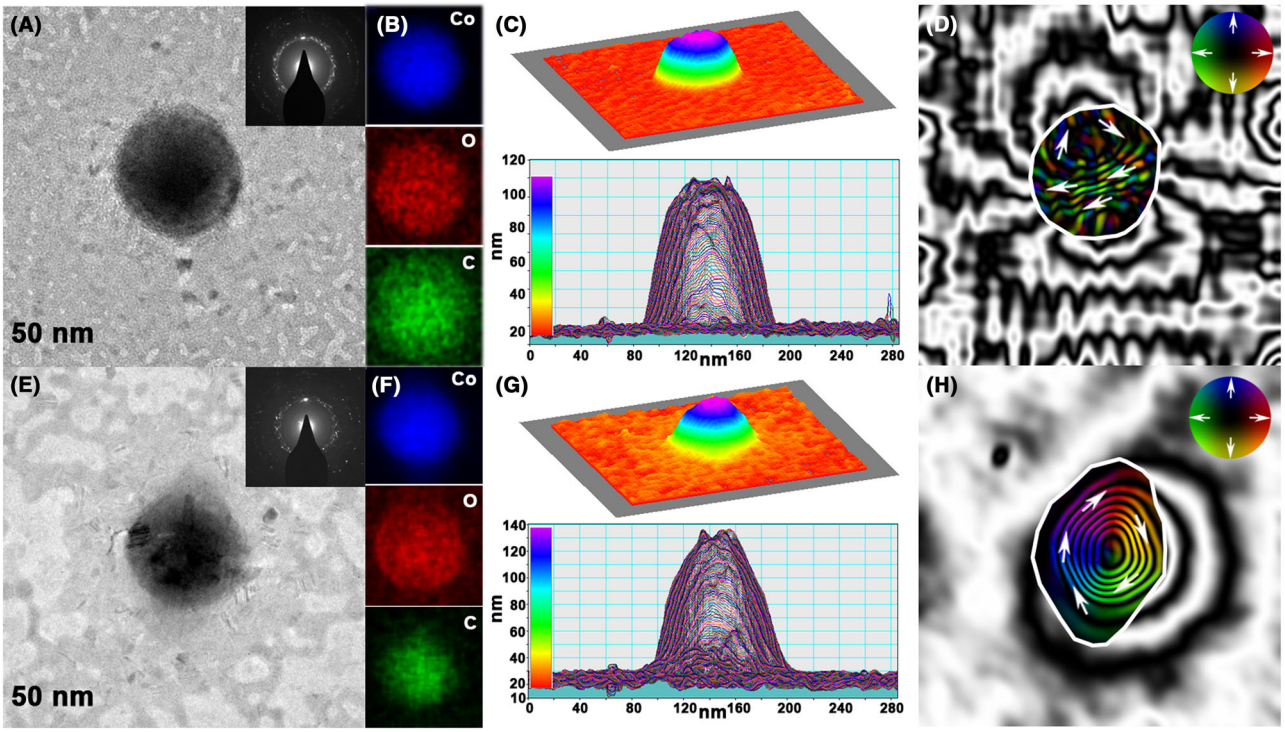

Fig. 1. (A, E) BF TEM images of a Co NP (A) before and (E) after *in situ* heating to 400°C, with SAED patterns (inset). (B, F) Associated EDX chemical maps showing the elemental distribution of cobalt, oxygen and carbon. (C, G) Morphology and thickness profile of the Co NP estimated from the ϕ_e and constant MIP. The colour in the top panel represents height and is defined by the scale bar in the thickness profile (bottom panel, inset). (D, H) Magnetic induction maps reconstructed from holograms acquired (D) before and (H) after *in situ* heating to 400°C. The contour spacing is (D) 0.049 and (H) 0.785 radians and magnetisation direction is shown using arrows, as depicted in the colour wheel.

Table 1. Quantification from the entire EDX chemical maps in Figures 1 and 2, before and after annealing.

	Co NP in Figure 1		Co NP in Figure 2	
Element	Preanneal atom%	Postanneal atom%	Preanneal atom%	Postanneal atom%
Carbon	51.9	26.4	50.1	25.4
Oxygen	24.5	30.8	23.9	28.0
Cobalt	13.1	25.8	16.6	29.0
Nitrogen	8.5	13.2	7.6	14.5
Silicon	2.0	3.6	1.8	3.1

of 50% of total atomic C% from the NP surface (Table 1), whilst Figure 2(G) reveals amplified overspray roughness, an increase in height of the Co NP by ~30 nm and widening of its base. The magnetic induction map of Figure 2(H) shows magnetic contours flowing from bottom to top through the Co NP with flux closure either side, indicative of a vortex core aligned along the vertical axis with a stray magnetic field.

Discussion

This TEM investigation has provided chemical, magnetic and structural characterisation of two Co NPs grown by FEBID and demonstrated the effect of *in situ* annealing to 400°C. It is clear the FEBID technique has successfully deposited two circular Co NPs ~90 nm in diameter on the SiN windows of the Wildfire e-chips, along with Co overspray. The as-grown Co NPs are found to be polycrystalline and EDX analysis reveals they include a significant amount of carbon. This is consistent with previous studies showing the deposits grown at similarly low electron beam current comprise small isolated cobalt nanocrystals (5–7 nm in size) embedded in an amorphous carbon matrix (Córdoba *et al.*, 2011). EDX analysis also confirms the formation of an oxide-rich shell around the highly-reactive Co NPs, considered due to exposure to ambient conditions after the FEBID process. Using the relationship $\phi_e = C_E V_0 t$ provides

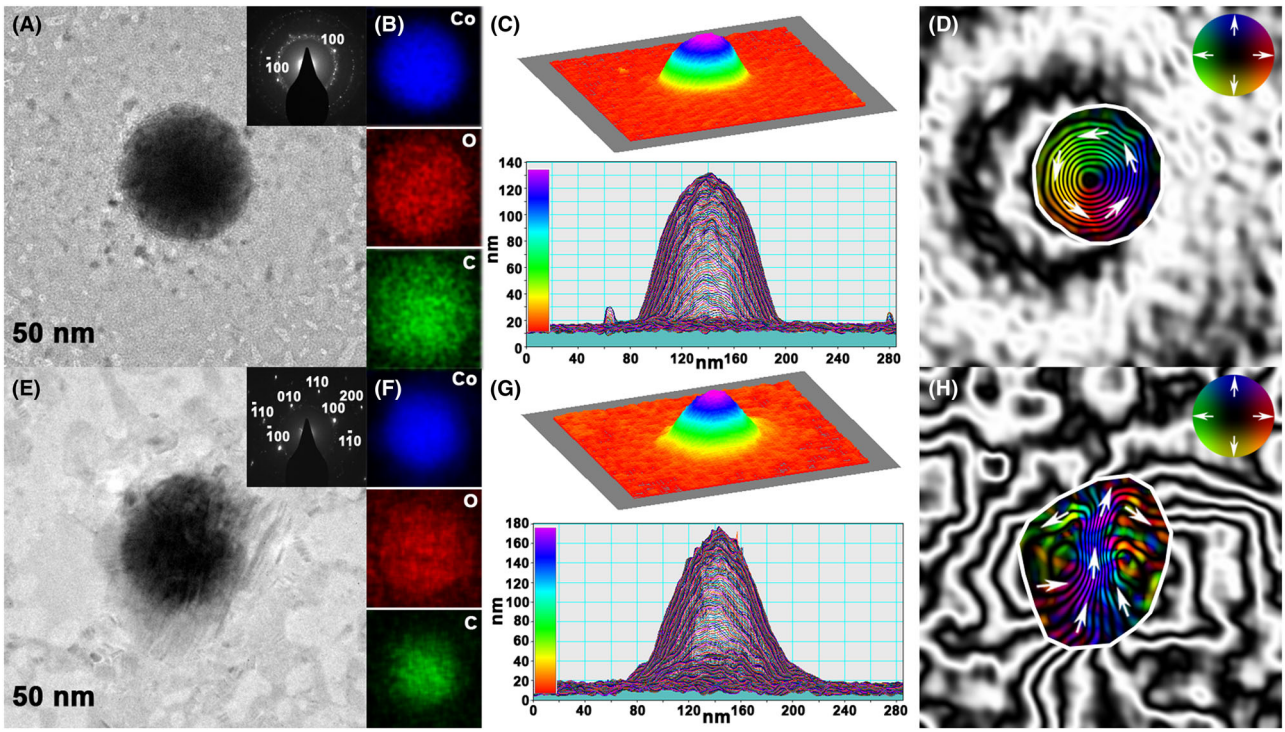

Fig. 2. (A, E) BF TEM images of a Co NP (A) before and (E) after *in situ* heating to 400°C, with SAED patterns (inset). (B, F) Associated EDX chemical maps showing the elemental distribution of cobalt, oxygen and carbon. (C, G) Morphology and thickness profile of the Co NP estimated from the ϕ_e and constant MIP. The colour in the top panel represents height and is defined by the scale bar in the thickness profile (bottom panel, inset). (D, H) Magnetic induction maps reconstructed from holograms acquired (D) before and (H) after *in situ* heating to 400˚C. The contour spacing is (D) 0.524 and (H) 0.131 radians and magnetisation direction is shown using arrows, as depicted in the colour wheel.

a useful method to visualise the morphology and thickness profile of the Co NPs, assuming they are grown with a flat base of the SiN membrane. This would perhaps not be appropriate for drop-cast nanoparticle powders. Whilst the two native Co NPs exhibit similar dimensions, the magnetic induction maps both reveal vortex states but at different orientations.

The *in situ* annealing to 400°C has had a significant effect on both Co NPs, most notably the increased roughness of the Co overspray and its apparent migration into the Co NPs. This has resulted in widening of their base, particularly in Figure 2(G), and an increase in their height by ~25–30 nm, assuming their V_0 does not change significantly with annealing. Another pronounced effect is concentration of the carbon signal in the EDX maps towards the centre of the Co NPs. *In situ* annealing has been shown to increase the relative Co content in FEBID grown nanostructures through coarsening growth of crystallites (Pablo-Navarro *et al.*, 2018) and is considered to induce C-diffusion from the Co NP surface, resulting in a 50% reduction in atomic C % for both NPs. This coarsening effect is confirmed by the SAED patterns, with Figure 2(E) (inset) suggesting the *in situ* annealing has promoted a single crystalline Co_3O_4 shell. The annealing also had a marked effect on the magnetic properties of the Co NPs, and it is considered the variation in remanent domain states are due to the morphology-dependent changes in shape anisotropy. The main difference between the magnetic induction maps in Figures 1 and 2 is that with annealing, the vortex states change from side-on view to a view a down the vortex core (Fig. 1), and vice versa (Fig. 2). Whilst annealing is known to increase the net magnetization strength in FEBID-grown Co nanostructures (Pablo-Navarro *et al.*, 2018), these changes in orientation of the magnetic states prevent direct comparison of quantitative measurements of in-plane induction. This is because electron holography is only sensitive to the in-plane component of the magnetic induction. Hence these differently oriented magnetic states could present a large proportion of magnetic induction either in-plane or out-of-plane by comparison, which would explain the difference in phase contours in the magnetic induction maps. The marked chemical and structural changes induced by annealing at 400°C imply the FEBID-grown NPs are not ideal candidates for investigating temperature induced changes in vortex domain states, which are known to be thermally stable up to relatively high temperatures (Nagy *et al.*, 2017). However, this study has demonstrated that *in situ* annealing can be used to improve the crystallinity and, with improved control, tune the net magnetization of individual NPs or large complex arrays produced by FEBID, for potential use in magnetic data storage.

In summary, FEBID has successfully grown isolated CS Co NPs ~90 nm on *in situ* TEM chips. Off-axis electron holography reveals their morphology, thickness and vortex magnetic domain states. *In situ* annealing induced migration of the Co-overspray to grow the Co NPs and increase their crystallinity, but their instability under heating restricts their suitability for examining thermally induced magnetic processes.

Acknowledgement

The authors thank the University of Glasgow (200540-01) and Carnegie Trust (RIG007390) for funding.

References

Almeida, T.P., Moro, F., Fay, M.W., Zhu, Y.Q. & Brown, P.D. (2014) Tuneable Magnetic Properties of Hydrothermally Synthesised Core / Shell $CoFe_2O_4$ / $NiFe_2O_4$ and $NiFe_2O_4$ / $CoFe_2O_4$ Nanoparticles. *J. Nanopart. Res.* **16**, 2395.

Almeida, T.P., Muxworthy, A.R., Kovács, A. *et al.* (2016) Direct observation of the thermal demagnetization of a vortex structure held by a non-ideal magnetite recorder. *Geophys. Res. Lett.* **43**, 8426–8434.

Almeida, T.P., Muxworthy, A.R., Kovács, A., Williams, W., Brown, P.D. & Dunin-Borkowski, R.E. (2016) Direct visualization of the thermomagnetic behaviour of pseudo-single-domain magnetite particles. *Sci. Adv.* **2**, e1501801.

Anishchenko, R.I. (1966) Calculation of the Mean Inner Potential of a Crystal in the Statistical Theory. *Phys. Stat. Sol.* **18**, 923.

Bernau, L., Gabureac, M., Erni, R. & Utke, I. (2010) Tunable Nanosynthesis of Composite Materials by Electron-Impact Reaction. *Angew. Chem. Int. Ed.* **49**, 8880–8884.

Chong, R.K.K., Dunin-Borkowski, R.E., Kasama, T., Hytch, M.J. & McCartney, M.R. (2003) Off-axis electron holography and image spectroscopy of ferromagnetic FeNi nanoparticles. *Inst. Phys. Conf. Ser.* **179**, 451–454.

Córdoba, R., Sesé, J., De Teresa, J.M. & Ibarra, M.R. (2010) High-purity cobalt nanostructures grown by focused-electron-beam-induced deposition at low current. *Microelectron. Eng.* **87**, 1550–1553.

Córdoba, R., Fernández-Pacheco, R., Fernández-Pacheco, A., Gloter, A., Magén, C., Stéphan, O., Ibarra, M.R. & De Teresa, J.M. (2011) Nanoscale chemical and structural study of Co-based FEBID structures by STEM-EELS and HRTEM. *Nanoscale Res. Lett.* **6**, 592.

De Teresa, J.M., Fernández-Pacheco, A., Córdoba, R., Serrano-Ramón, L., Sangiao, S. & Ibarra, M.R. (2016) Review of magnetic nanostructures grown by focused electron beam induced deposition (FEBID). *J. Phys. D: Appl. Phys.* **49**, 243003.

Dunin-Borkowski, R.E., McCartney, M.R., Smith, D.J. & Parkin, S.S.P. (1998) Towards quantitative electron holography of magnetic thin films using *in situ* magnetization reversal. *Ultramicroscopy* **74**, 61–73.

Fernández-Pacheo, A., De Teresa, J.M., Córdoba, R. & Ibarra, M.R. (2009) Magnetotransport properties of high-quality cobalt nanowires grown by focused-electron-beam-induced deposition. *J. Phys. D: Appl. Phys.* **42**, 055005.

Fernández-Pacheo, A., De Teresa, J.M., Córdoba, R. *et al.* (2009) Domain wall conduit behavior in cobalt nanowires grown by focused electron beam induced deposition. *Appl. Phys. Lett.* **94**, 192509.

Fernández-Pacheo, A., Serrano-Ramón, L., Michalik, J.M. *et al.* (2013) Three dimensional magnetic nanowires grown by focused electron-beam induced deposition. *Sci. Rep.* **3**, 1492.

Hÿtch, M.J., Dunin-Borkowski, R.E., Scheinfein, M.R., Moulin, J., Duhamel, C., Mazaleyrat, F. & Champion, Y. (2003). Vortex flux channeling in magnetic nanoparticle chains. *Phys. Rev. Lett.* **91**, 257207.

Lavorato, G.C., Lima Jr., E., Troiani, H.E., Zysler, R.D. & Winkler, E.L. (2015) Exchange-coupling in thermal annealed bimagnetic core/shell nanoparticles. *J. Alloys Compd.* **633**, 333–337.

Lee, J-H., Jang, J-t., Choi, J-s. *et al.* (2011) Exchange-coupled magnetic nanoparticles for efficient heat induction. *Nat. Nanotechnol.* **6**, 418–422.

Nagy, L., Williams, W., Muxworthy, A.R., Fabian, K., Almeida, T.P., Ó Conbhuí, P. & Shcherbakove V.P. (2017) Stability of equidimensional pseudosingle-domain magnetite over billion-year timescales. *PNAS* **114**, 10356–10360.

Pablo-Navarro, J., Magen, C. & de Teresa, J.M. (2018) Purified and Crystalline Three-Dimensional Electron-Beam-Induced Deposits: The Successful Case of Cobalt for High-Performance Magnetic Nanowires. *ACS Appl. Nano Mater.* **1**, 38–46.

Sanchez, A. & Ochando, M.A. (1985) Calculation of the mean inner potential. *J. Phys. C: Solid State Phys.* **18**, 33.

Serrano-Ramón, L., Córdoba, R., Rodríguez, L.A. *et al.* (2011) Ultrasmall functional ferromagnetic nanostructures grown by focused electron-beam-induced deposition. *ACS Nano.* **5**(10), 7781–7787.